Theoretical and Computational Fluid Dynamics manuscript No.
(will be inserted by the editor)

Ionut Danaila · Claudiu Vadean · Sterian Danaila

Specified discharge velocity models for numerical simulations of laminar vortex rings

Received: date / Accepted: date

Abstract We numerically and theoretically investigate the flow generated at the exit section of a piston/cylinder arrangement that is generally used in experiments to produce vortex rings. Accurate models for the velocity profile in this section (also called specified discharge velocity, SDV models) are necessary in *(i)* numerical simulations of laminar vortex rings that do not compute the flow inside the cylinder and *(ii)* in slug-models that provide a formula for the total circulation of the flow. Based on the theoretical and numerical analysis of the flow evolution in the entrance region of a pipe, we derive two new, and easy to implement, SDV models. A first model takes into account the unsteady evolution of the centerline velocity, while the second model also includes the time variation of the characteristics of the boundary layer at the exit plane of the vortex generator. The models are tested in axisymmetric direct numerical simulations of vortex rings. As distinguished from classical SDV model, the new models allow to accurately reproduce the characteristics of the flow. In particular, the time evolution of the total circulation is in good agreement with experimental results and previous numerical simulations including the vortex generator. The second model also provides a more realistic time evolution of the vortex ring circulation. Using the classical slug-model and the new correction for the centerline velocity, we finally derive a new and accurate analytical expression for the total circulation of the flow.

Keywords Vortex ring · Navier-Stokes equations · direct numerical simulation · cylindrical coordinates · inflow boundary condition · vortex ring · pipe flow · boundary layer · slug model

PACS 47.32.cf · 47.15.Uv · 47.27.ek

Ionut Danaila
UPMC Univ Paris 06, UMR 7598, Laboratoire Jacques-Louis Lions, F-75005, Paris, France
CNRS, UMR 7598, Laboratoire Jacques-Louis Lions, F-75005, Paris, France
Tel.: +33-1-44277169
Fax: +33-1-44277200
E-mail: danaila@ann.jussieu.fr

Claudiu Vadean
Faculty of Aerospace Engineering, Politechnica University, Calea Grivitei 132, Bucharest, Romania
Tel.: +40-214023967
Fax: +40-212129220
E-mail: c_vadean@aero.pub.ro

Sterian Danaila
Faculty of Aerospace Engineering, Politechnica University, Calea Grivitei 132, Bucharest, Romania
Tel.: +33-1-44277169
Fax: +33-1-44277200
E-mail: s_danaila@aero.pub.ro

1 Introduction

Vortex rings and, more generally, flows resulting from the sudden injection of fluid in a quiescent surrounding, are encountered in numerous practical applications, ranging from combustion to bio-mechanics, and synthetic jet actuators. This explains the growing interest of the scientific community in (re)exploring basic properties of this fundamental flow using modern experimental and numerical tools. Direct numerical simulations were systematically used to support recent experimental or theoretical investigations on the vortex ring formation [10], post-formation [4], circulation and trajectory [14], mixing [2], transport and stirring [30], etc. An important problem in numerical simulations of vortex rings is how to represent or model the vortex generator in order to accurately describe experimental configurations. The purpose of the present contribution is to address this issue and to derive an improved, but still easy to implement, analytical model describing the specified discharge velocity (SDV) profile that is commonly used to prescribe inflow boundary conditions in vortex ring numerical simulations.

Laminar vortex rings are usually produced in laboratory by pushing a column of fluid (by a piston/cylinder mechanism, e.g. [8], or a piston gun, e.g. [33]) through a long cylinder. The flow is assumed to be axisymmetric and thus easily described in cylindrical coordinates (z, r, θ), with z the longitudinal (propagation) direction of the flow. When the fluid enters the surrounding flow that is initially at rest, the generated cylindrical vortex sheet rolls-up into a vortex ring. The geometry at the edge of the cylinder defines the type of the vortex generator: orifice (Fig. 1a) or tube (Fig. 1b). The orifice generator can also be regarded as a cylindrical cavity in a plane wall – when the orifice area is smaller than the cylinder one, a new orifice configuration (not discussed here) with *vena contracta* is obtained (see for instance [16, 14]).

When considering orifice or tube configurations (Fig. 1a,b), the pipe flow developing in a cylinder of length L_e and diameter D is also simulated [9, 25, 12, 28, 10, 14]. At the entry of the cylinder, the axial velocity U_{P} is imposed and usually set equal to the piston velocity. An alternative numerical configuration (Fig. 1c) consists in removing the cylinder part and modelling the vortex ring generator by prescribing an appropriate axial velocity profile at the inflow boundary. This specified discharge velocity (SDV) configuration obviously requires a simpler geometry setting and reduced computational time. This explains why the SDV model is commonly used for the simulation of vortex rings [25, 11, 35, 4]. An equivalent approach to model the vortex generator was proposed by Mohseni *et al.* [21]. A long-duration non-conservative force was introduced in a small region at the entry of the computational domain in order to obtain in the center of the forcing region a velocity profile that resembles the experimental profile at the exit of a nozzle. Vortex rings similar to those generated by a piston/cylinder mechanism were thus obtained, but also thicker rings that are not associated to a particular geometry of the vortex generator. The present contribution focuses on classical SDV models for the piston/cylinder configuration.

In the commonly used SDV model, the inlet velocity U_{SDV} is the product of the piston velocity (depending on time t) with a basic velocity profile (depending on the radial coordinate r). The velocity profile takes into account the thickness of the vorticity layer at the cylinder lip. This model (described in detail in the next section) was successfully used in simulating laminar vortex rings [25, 11, 35, 4] with accurate prediction of the key features of the flow, as the main integrals of motion: circulation (Γ), hydrodynamic impulse (I) and energy (E). These quantities are defined for the case of axisymmetric motion as (e.g. [27]):

$$\Gamma = \int \omega dr dz, \quad I = \pi \int \omega r^2 dr dz, \quad E = \pi \int \omega \psi dr dz, \tag{1}$$

where ω is the (azimuthal) vorticity and ψ the corresponding Stokes stream function.

The total circulation of the flow obtained with the SDV model shows good agreement with experiments or numerical simulations of orifice/tube cases, if scaled with its maximum value (e.g. [35, 4]). When considering physical units, the SDV model gives lower values for the total circulation, as numerically shown for the first time by Rosenfeld, Rambod and Gharib [25] (henceforth denoted as RRG). Numerical data of RRG are also plotted in Fig. 9 that presents one of the main results of this paper. RRG also showed that numerical simulations of the orifice case provide values of the circulation closer to experimental results reported by Gharib, Rambod and Shariff [8](denoted as GRS). The explanation lies on the fact that the simulation of the cylinder part of the vortex generator allows to implicitly represent the unsteady evolution of the boundary layer characteristics at the cylinder lip. It follows that an improved SDV model has to take into account this phenomenon.

Based on the analysis of the flow evolution in the entrance region of a pipe, we suggest in this paper two new models (SDV models 2 and 3 in Fig. 9) by correcting the velocity U_{SDV} at two levels: by introducing the

unsteady evolution of its centerline value and by taking into account the unsteady evolution of the vorticity layer thickness. The former correction was discussed in [32,5], resulting in a simple model for the centerline velocity at the inlet. Using a similar model we derive a more accurate expression for the centerline velocity when compared to pipe-flow simulations. The latter point was not yet discussed in the literature and we show that it plays an important role in describing vortex ring trajectories and geometric characteristics.

The paper is organized as follows. The next section presents the numerical methodology used in this study. The analytical form of the commonly used SDV models is then introduced. Two new SDV models are derived in the main body of the paper and tested in vortex ring direct numerical simulations. Finally, some theoretical and computational implications of the improved SDV models are discussed.

2 Numerical methodology

The idea of the present study is to simulate the flow inside the vortex generator separately from the flow in the chamber where the vortex ring evolves. The former system is a classical laminar pipe-flow, whilst the latter is the SDV configuration illustrated in Fig. 1c. Both vortex ring and pipe flows are computed using the numerical code validated in [4] for the simulation of axisymmetric vortex rings.

The incompressible Navier-Stokes equations in cylindrical coordinates (r,θ,z) are solved using the numerical method proposed by Rai and Moin [24] and modified by Verzicco and Orlandi [34]. The method is described in great detail by Orlandi [22] (see also [26]). The equations are written in primitive variables $(r\cdot v_r, v_\theta, v_z)$ and solved on a staggered grid to avoid the problem of singularities introduced by the axis $r=0$. Second order finite differences are used for the spatial discretization. For the time advancement we use a fractional-step method [13] based on a combination of a low-storage third-order Runge–Kutta scheme for the convective terms and a semi-implict Crank–Nicolson scheme for the viscous terms. At each substep of the Runge–Kutta scheme, the momentum equations are solved by an approximate factorization technique [13] and a Poisson equation is solved for the pressure correction. The Poisson solver uses a fast Fourier transform following the azimuthal direction θ and an effective cyclic reduction method (Fishpack subroutines) for solving the remaining two-dimensional system following (r,z) directions. The method is globally second order accurate in space and time.

In the following, all presented quantities will be normalized using as length and velocity scales the diameter D of the pipe, and, respectively, the maximum (piston) velocity U_0 at the entry of the pipe. The corresponding reference time is thus D/U_0. Physical quantities, when referred, will be denoted by $\widetilde{()}$. The main physical parameter of the flow is the Reynolds number based on the characteristic velocity:

$$Re_{\mathrm{D}} = \frac{U_0 D}{\nu}. \tag{2}$$

We set $Re_{\mathrm{D}} = 2500$ for both vortex ring and pipe flows, as in the simulations of RRG.

For vortex ring simulations we use the same computational settings as in [4] where the long time evolution of a laminar vortex ring was accurately captured. The domain (Fig. 1c) extends radially to $R_d = 4$, which ensures a negligible influence of lateral slip-wall boundary on the dynamics of the vortex ring. The length of the domain is $L_d = 20$, avoiding the vortex ring to get close to the downstream boundary, where we apply a convective [23] boundary condition, enforced by a global mass conservation procedure [26]. The grid is uniform in the axial direction and stretched in the radial direction such that at least 30 grid points are clustered in the vorticity layer of the inflow axial velocity profile. In the following, all vortex ring simulations will employ a refined grid of 301×1251 points, for which the grid convergence of the results is ensured.

For pipe-flow simulations, a non-slip wall boundary condition is used for the lateral wall ($r=0.5$) where the grid is stretched following a hyperbolic tangent distribution law [22]. A zero velocity gradient boundary condition is imposed at the outlet. The pipe length is $L_e = 8$ and the grid has 101×401 points in the radial and, respectively, longitudinal directions. Test with a refined 201×801 grid showed grid independence of the results. The results obtained on the fine grid are used below to validate the analytical form of SDV models.

For both vortex-ring and pipe-flow simulations, time-step refinement tests showed negligible differences for $dt < 0.001$. We consequently used a fixed time-step of $dt = 0.001$, that is largely below the admissible value imposed by the stability of the numerical scheme.

3 SDV inflow boundary conditions for vortex ring simulations

For orifice or tube configurations (Fig. 1a,b), the axial velocity U_{P} imposed at the inlet of the cylinder of diameter D has the form:

$$U_{\text{P}}(t,r) = U_0\, F_{inj}(t)\, U_{\text{TH}}(r), \tag{3}$$

where U_0 is the maximum piston velocity and F_{inj} the piston motion law (ramp, trapezoidal, etc.) normalized to unity.

Since L_e is usually taken larger than the piston stroke L_{P}, most of the studies [25,12,28,10,14] consider a uniform (*i.e.* top-hat) profile to represent the spatial velocity profile $U_{\text{TH}}(r)$. A heuristic representation of the boundary-layer thickness in the cylinder was introduced in [9] to correct $U_{\text{TH}}(r)$, when simulating small cylinder lengths ($L_e \leq 2$).

For the SDV case (Fig. 1c), the velocity U_{SDV} models the velocity at the exit of the cylinder and is commonly imposed as:

$$\text{(SDV model 1)} \quad U_{\text{SDV}}(t,r) = U_0\, F_{inj}(t)\, U_b(r), \tag{4}$$

where the basic velocity profile $U_b(r)$ now takes into account for the finite thickness of the vorticity layer at the edge of the cylinder. The analytical expression of $U_b(r)$ is usually [11,35,4] given by the classical hyperbolic tangent form, which matches very well the shape of jet profiles measured in experiments (see e.g. [17]). We write here $U_b(r)$ in the form:

$$U_b(r) = \frac{1}{2}\left\{1 + \tanh\left[\frac{1}{4\Theta}\left(1 - \frac{r}{R_{jet}}\right)\right]\right\}, \tag{5}$$

where R_{jet} is the radius of the cylinder and Θ the (dimensionless) momentum thickness

$$\Theta = \int_0^\infty U_b\,(1 - U_b)\, dr. \tag{6}$$

The velocity profile $U_b(r)$ and the corresponding vorticity distribution $\omega = -\partial U_b/\partial r$ are plotted in Fig. 2a. The maximum of the vorticity is obtained for $r = R_{jet}$, corresponding to the inflexion point of the profile. The momentum thickness is directly related to the vorticity thickness by $\delta_\omega = 1/\omega_{max} = 4\Theta$ and plays the role, together with R_{jet}, of a control parameter of the shape of the profile. Note that R_{jet} and Θ are constants in the 'SDV model 1' (4).

The time variation of the SDV velocity in (4) is given by the product $U_0 \cdot F_{inj}(t)$ which is represented in Fig. 2b. In all following simulations, we consider the trapezoidal injection program proposed in [11] to describe the piston motion

$$F_{inj}(t) = \begin{cases} \dfrac{1}{2}\left\{1 + \tanh\left[\dfrac{5}{\tau_1}(t - \tau_1)\right]\right\}, & t \leq \tau_1 + \tau_2/2 \\ \dfrac{1}{2}\left\{1 + \tanh\left[\dfrac{5}{\tau_1}(\tau_1 + \tau_2 - t)\right]\right\}, & t > \tau_1 + \tau_2/2. \end{cases} \tag{7}$$

The constants τ_1 and τ_2 separate the three parts in the piston motion: acceleration for $t \in [0, \tau_1[$, velocity plateau for $t \in]\tau_1, \tau_2]$ and deceleration for $t \in]\tau_2, t_{\text{off}}]$. Considering small values for τ_1 ($\tau_1 = 0.15$ in Fig. 2b) we obtain sharp acceleration/deceleration phases as commonly used in experiments.

4 Improved SDV models

Using an analytical and numerical analysis of the flow evolution in the entrance region of a pipe, we derive in this section two new improved SDV models. Their behaviour will be estimated in the next section by direct numerical simulations of laminar vortex rings.

4.1 Unsteady flow evolution in the inlet region of a smooth pipe

The entrance region of a smooth pipe is generally divided in two parts: the inlet region, where the boundary layer is still thin, and the filled region, where the boundary layer reaches the axis, but the Poiseuille velocity profile is not yet developed (e.g. [7,19]). A more detailed analysis of the inlet region reveals the existence of two distinctive spatial zones, sketched in Fig. 3. In the region near the inflow section, region also called developing flow zone [32], the axial velocity profile has its maximum near the wall and not on the axis. This a consequence of the sudden pressure drop on the axis. The velocity evolves to a typical boundary-layer velocity profile in the downstream Stokes region. Since the vortex generator generally use large pipe lengths L_e compared to the piston stroke length L_p, we are concerned with the Stokes region analysis.

In the Stokes region, a first approximation of the pipe-flow is obtained by considering small times for which the flow could be separated into a 'free-stream' (pipe center) flow with constant velocity and a very thin boundary layer developing at the pipe wall. For $t \to 0$, the unsteady boundary layer equations are simplified by the fact that the unsteady term in the momentum equation is mainly balanced by the viscous diffusion along the radial direction (see [3], p. 322). Using dimensionless variables

$$y = \widetilde{y}/D, \quad u = \widetilde{u}/U_0, \quad t = \widetilde{t}/(D/U_0), \tag{8}$$

and the reference frame ($y = 0.5 - r$, z) attached to the pipe wall, the boundary-layer momentum equation reduces to

$$\frac{\partial u}{\partial t} = \frac{1}{Re_{\text{D}}} \frac{\partial^2 u}{\partial y^2}, \quad 0 \le y \le \delta, \tag{9}$$

with initial and boundary conditions:

$$\begin{cases} t = 0 : u = 0 \quad \text{for all} \quad 0 \le y \le \delta, \\ t > 0 : u = 0 \quad \text{for} \quad y = 0 \quad \text{and} \quad u = U_{\text{CL}} \quad \text{for} \quad y = \delta, \end{cases} \tag{10}$$

where U_{CL} is the centerline velocity (which can be a function of z) and δ the thickness of the boundary layer (see Fig. 3). The solution of (9) and (10) is expressed in [29] (p. 92), for the similar problem of flow formation in Couette motion, as a series of complementary error function:

$$\frac{u(y,t)}{U_{\text{CL}}} = 1 - \sum_{n=0}^{\infty} \text{erfc}\left[2n\eta_1 + \eta\right] + \sum_{n=0}^{\infty} \text{erfc}\left[(2n+1)\eta_1 - \eta\right], \tag{11}$$

where

$$\eta = \frac{y}{B(t)}, \quad \eta_1 = \frac{\delta}{B(t)}, \tag{12}$$

with

$$B(t) = \frac{2}{\sqrt{Re_{\text{D}}}} \sqrt{t}. \tag{13}$$

If $B(t)$ is considered small, a good approximation of the velocity profile is obtained by keeping only the first term in the series expansions

$$\frac{u(y,t)}{U_{\text{CL}}} = 1 - \text{erfc}(\eta) = \text{erf}\left(\frac{y}{B(t)}\right). \tag{14}$$

It should be noted that (14) is the exact solution of (9) with the boundary condition $U = U_{\text{CL}}$ for $y \to \infty$, that could be considered as an asymptotic matching condition of the boundary-layer velocity with the potential core velocity developing near the axis of symmetry of the pipe ($u/U_{\text{CL}} = 1$ for $\delta \le y \le 0.5$). The velocity distribution (14) is the same as that obtained for a semi-infinite wall moving in infinite fluid with constant velocity $-U_{\text{CL}}$. The latter problem is referred as the first Stokes problem in [29] (p. 90).

The approximation (14) allows to extract the main properties of the boundary layer, as the modified displacement thickness

$$\delta^*(t) = \int_0^\delta \left(1 - \frac{u(y,t)}{U_{\text{CL}}}\right)(1-2y)\,dy, \tag{15}$$

and modified momentum thickness

$$\Theta^*(t) = \int_0^\delta \frac{u(y,t)}{U_{\text{CL}}}\left(1 - \frac{u(y,t)}{U_{\text{CL}}}\right)(1-2y)\,dy. \tag{16}$$

These quantities appear when writing the integral form of the boundary layer equations for axisymmetric configurations (e.g. [19]). In particular, the mass conservation equation takes the simple form :

$$\pi\frac{D^2}{4}U_0 = \pi\frac{D^2}{4}U_{\text{CL}} - \pi D(\delta^* D)U_{\text{CL}}. \tag{17}$$

Plugging (14) into the general definitions (15) and (16) with the approximation $\int_0^\delta \approx \int_0^\infty$ (valid since $u(y,t)/U_{\text{CL}} \approx 1$ for $y \geq \delta$), we obtain after some algebra (see Appendix A for the expressions of some useful definite integrals with erf function):

$$\delta^*(t) = \frac{B(t)}{\sqrt{\pi}} - \frac{B(t)^2}{2} \tag{18}$$

and

$$\Theta^*(t) = \frac{\sqrt{2}-1}{\sqrt{\pi}}B(t) - \frac{B(t)^2}{\pi}. \tag{19}$$

The centerline velocity results immediately from (17); using the expressions (18) and (13) we finally obtain:

$$U_{\text{CL}}(t) = \frac{U_0}{1-4\delta^*} = \frac{U_0}{1 - \dfrac{8}{\sqrt{\pi Re_{\text{D}}}}\sqrt{t} + \dfrac{8}{Re_{\text{D}}}t} \tag{20}$$

Note that the approximate model (9) was first used in [32, 5] to express the centreline velocity evolution $U_{\text{CL}}(t)$. Using several approximations (e. g. the axial-symmetry was not taken into account in the mass conservation equation) it was obtained in [5] that:

$$U_{\text{CL}}(t) = U_0\left(1 + \frac{8}{\sqrt{\pi Re_{\text{D}}}}\sqrt{t}\right). \tag{21}$$

In order to estimate the validity of this simple model and to compare the expressions (20) and (21) we perform pipe-flow simulations of the same configuration as in [32]. The numerical setting was described in section 2. The impulsive start of the flow generates two distinctive spatial zones in the pipe, which can be separated by monitoring the evolution of the centerline velocity U_{CL} versus the axial coordinate z. Figure 4 illustrates the characteristics of these zones for the time instant $t = 4$. In the developing region (a), near the inlet, the axial velocity profile has its maximum near the wall and not on the axis. The centerline velocity monotonically increases with z to its maximum value, reached in the Stokes region (b). In this last region the centerline velocity is constant with z and the thickness of the boundary layer is uniform. This is also the domain where the model (14) applies, since the hypothesis of a velocity profile not depending on the axial coordinate z is satisfied. Figure 4 also allows to visualize the propagation in time of the separation front between the two zones. The spatial extent of the Stokes zone is reduced in time, to finally disappear at $t = 8$.

The validity of the approximations (20) and (21) is estimated by using a 'temporal' analysis of the flow. Figure 5 shows the time evolution of the centerline velocity U_{CL} at different streamwise locations. For a given cross section of the pipe, the flow evolves from a Stokes configuration to a developing configuration. The initial temporal growth of the centerline velocity follows very well the law (20), until the front of the developing region reaches the given streamwise position. It should be noted that our model (20) considerably

improves the estimation of U_{CL} compared to the model (21) of Dabiri and Gharib, especially for long injection times.

The theoretical predictions (18) and (19) of the characteristics of the boundary layer in the Stokes region are also very well verified by the direct numerical simulations (Fig. 6). The modified displacement and momentum thickness are computed in simulations by using their expressions (15) and (16), modified for the developing region by replacing U_{CL} with the maximum value of the velocity profile. Figure 6 also allows to estimate the validity limit of the model. If the section $z = 6$ is considered as the exit section of the vortex generator, as in [32], the Stokes layer description is valid for injection times $t < 5.7$. This limit corresponds to a 2% relative error between model prediction and numerical data. Using the same criterion, we plot in Fig. 7 the time-limit t_d of our model for different axial sections. The linear increase of t_d with the axial distance z is also observed for lower Reynolds numbers ($Re_{\text{D}} = 800$). Since for an impulsive motion of the piston, the non-dimensional time is equivalent to the stroke ratio L_{P}/D, data from Fig. 7 could be used to calculate for an experimental device the minimum length of the cylinder for a given stroke ratio.

4.2 New SDV models

If the flow at the exit section of the vortex generator has a Stokes boundary layer configuration, the first idea in improving the SDV model (4) is to take into account the time variation of the centerline velocity. We obtain the

$$\text{(SDV model 2)} \quad U_{\text{SDV}}(t,r) = U_{\text{CL}}(t)\, F_{inj}(t)\, U_b(r), \tag{22}$$

where $U_{\text{CL}}(t)$ is given by our model (20) and $U_b(r)$ is the velocity profile (5) with constant vorticity layer thickness.

A further improvement of the SDV model is to take into account the time variation of the boundary layer characteristics at the exit section. For this purpose, the equivalence between the commonly used jet profile (5) and the boundary layer profile (14) is calculated. For the profile (14) the equivalent momentum thickness Θ is easily obtained (see also Appendix A),

$$\Theta(t) = \frac{\sqrt{2}-1}{\sqrt{\pi}}\, B(t) \tag{23}$$

and the jet radius R_{jet} is calculated by imposing that $u/U_{\text{CL}} = 0.5$ at $r = R_{jet}$:

$$R_{jet}(t) = \frac{1}{2} - 0.477\, B(t). \tag{24}$$

The expression of the third SDV model finally reads:

$$\text{(SDV model 3)} \quad U_{\text{SDV}}(t,r) = U_{\text{CL}}(t)\, F_{inj}(t)\, U_b(r,t), \tag{25}$$

where in the expression (5) of U_b we introduce the time variation of Θ and R_{jet} given by (23) and, respectively, (24).

Figure 8 compares velocity profiles extracted at $z = 6$ from the pipe-flow numerical simulation with model approximations (22) and (25). While both SDV models 2 and 3 reproduce correctly the increase in time of the centerline velocity value, only the SDV model 3 follows the increase of the momentum thickness of the profile and the diminishing of the equivalent jet radius. This last parameter, which remains constant ($R_{jet} = 0.5$) for the SDV model 2, was proved to play an important role in the evolution of the vortex ring (as discussed in [6] for vortex ring generators with variable exit diameters).

5 Numerical evaluation of the SDV models

Direct numerical simulations of laminar vortex ring are performed in this section using the SDV configuration (Fig. 1c). The numerical method and the axisymmetric computational domain were depicted in section 2. At the inlet we use successively the three SDV models (4), (22) and (25) to impose the axial velocity. The injection program (7) with $\tau_1 = 0.15$ and $\tau_2 = 5.95$ (Fig. 2b) corresponds to an equivalent stroke length $L_{\text{P}}/D = 6$ for a cylinder/piston vortex generator. This allows to compare the results with previously published data

(Fig. 9) for the same stroke length. The SDV models 1 and 2 use a velocity profile U_b with fixed momentum thickness $\Theta = 0.0125$ ($\delta_\omega = 0.05$).

Figure 9 displays the time evolution of the total circulation Γ of the flow, obtained from (1) by integrating the vorticity over the entire computational domain. The 'SDV model 1' (also used in [4]) gives similar results to the numerical results of RRG [25] obtained using an inlet boundary condition with impulsive injection program and top-hat velocity profile. Our results are superimposed to those of Zhao *et al.* [35] who used a very similar SDV model. The only difference, observed when the injection is stopped (*i.e.* at $t_{\text{off}} \approx 6$), is due to the fact that an injection program with a sharper deceleration was used in [35]. The circulation decrease at t_{off} comes from the existence of a zone of negative vorticity developing in the inlet wall boundary layer. In order to compare to experimental data of GRS [8], this zone near the inlet ($z \leq 0.2$) will be discarded from the integral used to compute the total circulation for the SDV cases 2 and 3 (see also [35]).

The correction (20) of the centerline velocity in SDV models 2 and 3 allows to fit closely experimental results [8] and numerical simulations of the orifice case [25,28]. The agreement is very good (Fig. 9) for the injection phase ($t < t_{\text{off}}$) and during the early period after the piston stops. The fast decrease of the total circulation in the results of Sau and Manesh [28], contrasting with our results and those of RRG, could come from the inclusion in the circulation integral of the stopping vortex that forms at the inlet. It should be noted that no particular model was used for the termination of the injection process, since we deal with long time injections that stop suddenly (Fig. 2b). Under these conditions, the stopping vortex normally travels back into the vortex generator and does not interact with the vortex ring (see the discussion in [14]), a phenomenon that could not be reproduced in SDV simulations.

The fact that the total circulation evolution is identical for the SDV models 2 and 3 could be easily explained using the so-called slug-model [31,16]. This model assumes that on the exit plane of the vortex generator the flow is parallel and that the rate of change of the circulation is given by the vorticity flux across this plane. It results that during the injection phase ($t < t_{\text{off}}$), the total circulation is approximated by

$$\Gamma_{slug}(t) = \frac{1}{2}\int_0^t U_{\text{CL}}^2(\tau)\, d\tau. \tag{26}$$

An improved slug-model taking into account the complete form of the vorticity flux across the exit plane was proposed in [15] and numerically validated in [14]. Since both SDV models 2 and 3 use the same expression (20) for $U_{\text{CL}}(t)$, one could expect to obtain the same total circulation during the injection phase. It is interesting to note that even after the injection stops, the decrease rate of the total circulation is almost the same for the SDV cases 2 and 3.

The difference between SDV models 2 and 3 is visible when analyzing the evolution of the vortex ring after t_{off}. For this purpose we separate the leading vortex ring from the flow as follows: the center C of the vortex is first located as the point of maximum vorticity ω_{max}; the vortex core is then defined as the inner domain bounded by the vorticity contour line $\omega/\omega_{max} = 0.05$ that encircles the center C. When the separation is not well-defined, this contour line is truncated and closed at the downstream location of the center of the vortex (see also [4]).

Figure 10 shows that immediately after the injection termination ($8 < t < 12$), the SDV models 2 and 3 provide almost the same vortex ring circulation Γ_{VR}. These values are in good agreement with previous numerical [25] and experimental results [8]. During this time period, the vortex ring is not completely formed and is still entraining fluid from its tail. For $t > 12$ the vortex ring obtained with SDV model 2 displays larger circulation values, while the SDV model 3 follows closely the results of RRG for the orifice case. The vortex ring circulation attains its maximum value Γ_{VR}^{max} at approximately the same time instant ($t_m = 14$) for both cases. At this time the vortex ring saturates and pinches-off from its wake. When reported to the time evolution of the total circulation (Fig. 9), the value Γ_{VR}^{max} is produced by the vortex generator at a time instant t_f called 'formation-time' [8]. The formation number value was reported to range from 3.6 to 4.5 for a variety injection conditions and is considered as an universal scale for the laminar vortex ring evolution. It can be seen by combining figures 9 and 10 that the value of the formation time strongly depends on the considered value of the vortex ring circulation. Using Γ_{VR}^{max} as reference value, we obtain in this study lower values (compared to the results of RRG) of the formation time t_f, but still in the admissible range (3.5 for SDV1, 3.4 for SDV2 and 3.8 for SDV3).

The difference between the SDV models 2 and 3 could be relevant if a precise description of the vortex ring is required. This could be interesting, for example, in applications using the vortex ring as combustion kernel for the ignition of a combustible mixture. To illustrate these differences, we plot in Fig. 11a) the time evolution of the radial coordinate R_v of the vortex ring center C. The vortex ring obtained with the SDV model

3 evolves closer to the axis of symmetry where vorticity cancellation occurs [11,25]. This explains its lower circulation in Fig. 10 compared to the vortex ring obtained with the SDV model 2. We recall that SDV models 2 and 3 use an injection program with larger centerline velocities than the SDV model 1 (Fig. 7), resulting in faster travelling vortex rings. We therefore compare in the following the characteristics of the SDV2 and SDV3 vortex rings, extracted at a time instant ($t = 14$) close to the pinch-off. Figure 11b displaying iso-contours of the vorticity shows that the topology of the two vortex rings is similar, with the vortex center shifted in both radial and longitudinal directions. It is interesting to observe that the maximum value of the vorticity in the center of the vortex is almost the same for the two cases (Fig.11c). Finally, we plot in Fig.11d the vortex ring signature $V(\psi)$ introduced in [18] to identify a vortex ring without swirl. This topological invariant is defined as the volume inside the torus $\psi = cst.$, where ψ is the Stokes stream function in the frame moving with the vortex ring (see also [4]). Since $\psi = 0$ defines the vortex bubble (or atmosphere), $V(0)$ is the volume of the vortex bubble. We observe that the two vortices have similar signatures; the SDV2 vortex has a larger bubble volume than the SDV3 vortex because of its larger diameter.

A final quantitative assessment of the SDV models is given by computing the normalized energy [8,20, 21] or normalized circulation [20,21] of the vortex ring after the pinch-off:

$$E^*_{\rm VR} = E_{\rm VR}/(I^{1/2}_{\rm VR}\Gamma^{3/2}_{\rm VR}), \quad \Gamma^*_{\rm VR} = \Gamma_{\rm VR}/(I^{1/3}_{\rm VR}W^{2/3}_{\rm VR}), \tag{27}$$

It was shown [20,21] that each vortex ring generator has a specific rate for feeding the flow with the kinetic energy, impulse, circulation, resulting in specific values for $E^*_{\rm VR}$ and $\Gamma^*_{\rm VR}$. For the three SDV models tested numerically, the values of $E^*_{\rm VR}$ and $\Gamma^*_{\rm VR}$ are very close, ranging from 0.27 to 0.3 and 2.05 to 2.12, respectively. These values are consistent with previously experimental and theoretical studies suggesting two universal scales ($E^*_{\rm VR} \approx 0.3$, $\Gamma^*_{\rm VR} \approx 2$) for vortex rings generated by a piston/cylinder mechanism [21]. Larger values for the normalized circulation were generated by [21] using numerical configurations analogous to an accelerated motion of the piston or a cylinder with time-variable diameter.

6 Summary and discussion

We show in this paper that accurate numerical simulations of laminar vortex rings can be performed without computing the flow inside the vortex ring generator. Similar results to experimental data and numerical data using the complete configuration are obtained when accurate models are used to prescribe the discharge velocity $U_{\rm SDV}$.

Compared to the classical specified discharge velocity (SDV1) model, we have derived and numerically tested two new models based on a simple theoretical analysis of the unsteady pipe-flow evolution. The model (SDV2) takes into account the unsteady evolution of the centerline velocity $U_{\rm CL}$, while the model (SDV3) also includes the time variation of the characteristics of the boundary layer at the exit plane of the vortex generator.

The model describing the time evolution of the parameters defining SDV profiles is valid only if the exit section of the vortex generator remains in the Stokes layer region of the pipe-flow. This region is characterized by very thin boundary layers and consequently axial velocity profiles are well approximated by the 'erf' profile (14). Nevertheless, this profile is representative for a boundary layer if the similarity variable $B(t)$ is small enough. Since $B(t)$ is expressed by (13), we infer that the model is valid for relatively large Reynolds numbers ($Re_{\rm D}$) of the flow and small injection times. The last condition is satisfied in the case of a vortex generator using a piston/cylinder mechanism when the piston stroke length $L_{\rm P}$ remains small compared to the length L_e of the cylinder. This seems to be the case in most experimental devices.

The centerline velocity correction (20) improves the model of Dabiri and Gharib [5] when compared to direct numerical simulations of pipe-flows (Fig. 5). As a direct consequence, the total circulation predictions derived from the slug-model (26) will also be affected. Since the slug-model is largely used in practical applications, we give below the closed forms for the circulation prediction

• using our model (20)

$$\Gamma(t) = \frac{U_0^2 Re_{\rm D}}{32\beta^2}\left[\frac{B(t)(B(t)-\alpha)}{(B(t)-\alpha)^2+\beta^2} + \frac{\alpha}{\beta}\arctan\left(\frac{B(t)\beta}{\frac{1}{2}-\alpha B(t)}\right)\right], \quad \alpha = \frac{1}{\sqrt{\pi}}, \quad \beta = \sqrt{\frac{1}{2}-\frac{1}{\pi}} \tag{28}$$

• and the model (21) of Dabiri and Gharib [5]:

$$\Gamma_{\rm DG}(t) = \frac{U_0^2 Re_{\rm D}}{8}[B(t)]^2\left[1+\frac{16}{3\sqrt{\pi}}B(t)+\frac{8}{\pi}[B(t)]^2\right] \tag{29}$$

In order to compare these slug-models, we performed vortex ring simulations using at the inflow section ($z = 0, r \leq 0.5$) the velocity profiles previously computed by pipe-flow direct numerical simulation with the same time-step and the same physical parameters ($Re_{\rm D}$, $L_{\rm p}/D$). Inflow velocity was extended with zero values outside the orifice ($r > 0.5$). The under-estimation of the centerline velocity by the model of Dabiri and Gharib observed in Fig. 5 results in lower values for the total circulation when using the slug-model. This effect is important when low Reynolds numbers and/or long time flow injections are considered, as shown in Fig. 12. It is also important to note that accurate estimation of the centerline velocity is also important in improved slug-models [15,14] that use $U_{\rm CL}(t)$ as a key input parameter.

The correction of the centerline velocity proved crucial to obtain values of the total circulation similar to those reported from experiments or numerical simulations of orifice configurations. Models SDV2 and SDV3 provided the same time evolution of the total circulation. Vortex ring circulations are in exchange different. The vortex ring simulated with the SDV3 model has a circulation closer to that obtained by RRG [25] for the case of an orifice configuration. This is not surprising, since in the SDV3 model the equivalent jet radius decreases in time, as in real orifice configurations. As a consequence, the SDV3 vortex ring evolves closer to the axis of symmetry than the SDV2 vortex. This explains the lower circulation and bubble volume of the SDV3 vortex.

Finally, it is important to remark that, unlike the classical SDV model, our models also include the Reynolds number dependance of the flow evolution. Further numerical simulations using the SDV3 model revealed the same Reynolds dependance as reported by RRG [25] for orifice configurations: as the Reynolds number decreases, the centerline velocity (20) increases and, consequently, the total circulation increases.

A Expressions of some definite integrals with error function

The properties of the error function

$$\mathrm{erf}(z) = \frac{2}{\sqrt{\pi}} \int_0^z e^{-t^2}\, dt, \tag{30}$$

are presented in great detail in [1], Chapter 7. Using the form of the indefinite integral

$$\int \mathrm{erf}(z) dz = \frac{e^{-z^2}}{\sqrt{\pi}} + z\,\mathrm{erf}(z), \tag{31}$$

the asymptotic expansion for $z \to \infty$

$$\mathrm{erf}(z) \sim 1 - \frac{e^{-z^2}}{\sqrt{\pi} z} \left(1 - \frac{1}{2z^2} + \frac{1\cdot 3}{(2z^2)^2} - \frac{1\cdot 3\cdot 5}{(2z^2)^3} + \ldots \right), \tag{32}$$

and the expressions of the integrals

$$\int_0^\infty z^{2n+1} e^{-az^2}\, dz = \frac{n!}{2a^{n+1}}, \tag{33}$$

$$\int_0^\infty z^{2n} e^{-az^2}\, dz = \frac{1\cdot 3\cdot \ldots (2n-1)}{2^{n+1} a^n} \sqrt{\frac{\pi}{a}}, \quad (a > 0, n = 0,1,2,\ldots), \tag{34}$$

we derived the following definite integrals, used to calculate integral quantities in section 4.1:

$$\int_0^\infty (1 - \mathrm{erf}(z))\, dz = \frac{1}{\sqrt{\pi}}, \quad \int_0^\infty (1 - \mathrm{erf}(z))^2\, dz = \frac{2 - \sqrt{2}}{\sqrt{\pi}}, \tag{35}$$

$$\int_0^\infty (1 - \mathrm{erf}(z))\, z dz = \frac{1}{4}, \quad \int_0^\infty \mathrm{erf}(z)(1 - \mathrm{erf}(z))\, dz = \frac{\sqrt{2} - 1}{\sqrt{\pi}}, \tag{36}$$

$$\int_0^\infty \mathrm{erf}(z)(1 - \mathrm{erf}(z))\, z dz = \frac{1}{2\pi}. \tag{37}$$

Acknowledgements We acknowledge the anonymous referee of our paper [4] who suggested in his report the idea of an imposed velocity profile with vorticity thickness depending on time.

References

1. Abramowitz, M., Stegun, I.A.: Handbook of mathematical functions with formulas, graphs and mathematical tables. National Bureau of Standards, Dover, New York (1972)
2. Archer, P.J., Thomas, T.G., Coleman, G.N.: Passive scalar mixing in vortex rings. J. Fluid Mech. **598**, 201-226 (2008)
3. Batchelor, G.K.: An Introduction to Fluid Dynamics, 7th edn. Cambridge University Press, Cambridge, New York (1988)
4. Danaila, I., Hélie, J.: Numerical simulation of the postformation evolution of a laminar vortex ring. Phys. Fluids **20**, 073602 (2008)
5. Dabiri, J.O., Gharib, M.: A revised slug model boundary layer correction for starting jet vorticity flux. Theor. Comput. Fluid Dynamics **17**, 293–295 (2004)
6. Dabiri, J.O., Gharib, M.: Starting flow through nozzles with temporally variable exit diameter. J. Fluid Mech. **538**, 111–136 (2005)
7. Fargie, D., Martin, B.W.: Developing laminar flow in a pipe of circular cross–section. Proceedings of the Royal Society of London. Series A, Mathematical and Physical Sciences **321**, 461–476 (1971)
8. Gharib, M., Rambod, E., Shariff, K.: A universal time scale for vortex ring formation. J. Fluid Mech. **360**, 121–140 (1998)
9. Heeg, R.S., Riley, N.: Simulations of the formation of an axisymmetric vortex ring. J. Fluid Mech. **339**, 199–211 (1997)
10. Hettel, M., Wetzel, F., Habisreuther, P., Bockhorn, H.: Numerical verification of the similarity laws for the formation of laminar vortex rings. J. Fluid Mech. **590**, 35–60 (2007)
11. James, S., Madnia, C.K.: Direct numerical simulation of a laminar vortex ring. Phys. Fluids **8**, 2400–2414 (1996)
12. Jiang, H., Grosenbaugh, M.A.: Numerical simulation of vortex ring formation in the presence of background flow with implications for squid propulsion. Theor. Comput. Fluid Dynamics **20**, 103–123 (2006)
13. Kim, J., Moin, P.: Application of a fractional step method to incompressible navier–stokes equations. J. Comput. Physics **59**, 308–323 (1985)
14. Krueger, P.S.: Circulation and trajectories of vortex rings formed from tube and orifice openings. Physica D **237**, 2218–2222 (2008)
15. Krueger, P.S., Gharib, M.: An over–pressure correction to the slug model for vortex ring calculation. J. Fluid Mech. **545**, 427–443 (2005)
16. Lim, T.T., Nickels, T.B.: Vortex rings, vol. Vortices in Fluid Flows, p. 95. Kluwer (1995)
17. Michalke, A.: Survey on jet instability theory. Prog. Aerospace Sci. **21**, 159–199 (1984)
18. Moffatt, H.K.: Generalised vortex rings with and without swirl. Fluid Dyn. Res. **3**, 22–30 (1988)
19. Mohanty, A.K., Asthana, S.B.L.: Laminar flow in the entrance region of a smooth pipe. J. Fluid Mech. **90**, 433–447 (1978)
20. Mohseni, K., Gharib, M.: A model for universal time scale of vortex ring formation. Phys. Fluids **10**, 2436–2438 (1998)
21. Mohseni, K., Ran, H., Colonius, T.: Numerical experiments on vortex ring formation. J. Fluid Mech. **430**, 267–282 (2001)
22. Orlandi, P.: Fluid Flow Phenomena: A Numerical Toolkit. Kluwer Academic Publishers, Dordrecht (1999)
23. Orlanski, I.: A simple boundary condition for unbounded hyperbolic flows. J. Comput. Physics **21**, 251–269 (1976)
24. Rai, M., Moin, P.: Direct simulations of turbulent flow using finite–difference schemes. J. Comput. Physics **96**, 15–53 (1991)
25. Rosenfeld, M., Rambod, E., Gharib, M.: Circulation and formation number of a laminar vortex ring. J. Fluid Mech. **376**, 297–318 (1998)
26. Ruith, M.R., Chen, P., Meiburg, E.: Development of boundary conditions for direct numerical simulations of three–dimensional vortex breakdown phenomena in semi–infinite domains. Computers & Fluids **33**, 1225–1250 (2004)
27. Saffman, P.G.: Vortex Dynamics. Cambridge University Press, Cambridge, New York (1992)
28. Sau, R., Mahesh, K.: Passive scalar mixing in vortex rings. J. Fluid Mech. **582**, 449–461 (2007)
29. Schlichting, H.: Boundary–Layer Theory. McGraw–Hill, New York (1979)
30. Shadden, S.C., Katija, K., Rosenfeld, M., Marsden, J.E., Dabiri, J.O.: Transport and stirring induced by vortex formation. J. Fluid Mech. **593**, 315-331 (2007)
31. Shariff, K., Leonard, A.: Vortex rings. Ann. Rev. Fluid Mech. **24**, 235–279 (1992)
32. Shusser, M., Gharib, M., Rosenfeld, M., Mohseni, K.: On the effect of pipe boundary layer growth on the formation of a laminar vortex ring generated by a piston–cylinder arrangement. Theor. Comput. Fluid Dynamics **15**, 303–316 (2002)
33. Sullivan, I.S., Niemela, J.J., Hershberger, R.E., Bolster, D., Donnelly, R.J.: Dynamics of thin vortex rings. J. Fluid Mech. **609**, 319-347 (2008)
34. Verzicco, R., Orlandi, P.: A finite–difference scheme for three–dimensional incompressible flows in cylindrical coordinates. J. Comput. Physics **123**, 402–414 (1996)
35. Zhao, W., Steven, H.F., Mongeau, L.G.: Effects of trailing jet instability on vortex ring formation. Phys. Fluids **12**, 589–596 (2000)

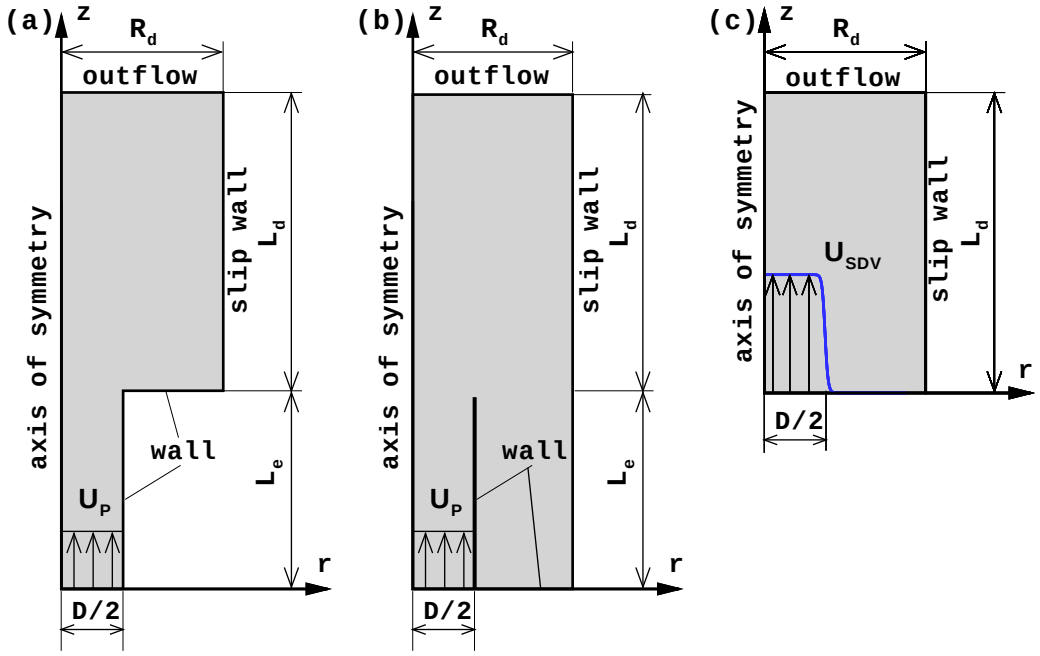

Fig. 1 Sketch of computational domains for vortex ring simulations: (a) orifice, (b) tube and (c) specified discharge velocity (SDV) configurations.

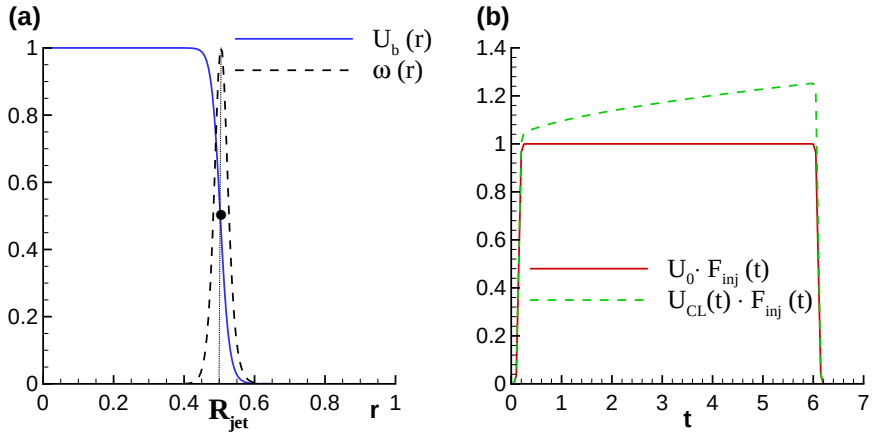

Fig. 2 (a) Velocity profile $U_b(r)$ modeled by the hyperbolic tangent law (5) for $\Theta = 0.0125$ ($\delta_\omega = 0.05$). The corresponding vorticity distribution ω, normalized by its maximum value, is also shown. The cylinder lip is located at $R_{jet} = 0.5$. (b) Time variation of the centerline velocity for the SDV model: model 1 (solid line) and model 2 or 3 (dashed line). The injection program F_{inj} is normalized to unity and given by equation (7) with $\tau_1 = 0.15$ and $\tau_2 = 5.95$.

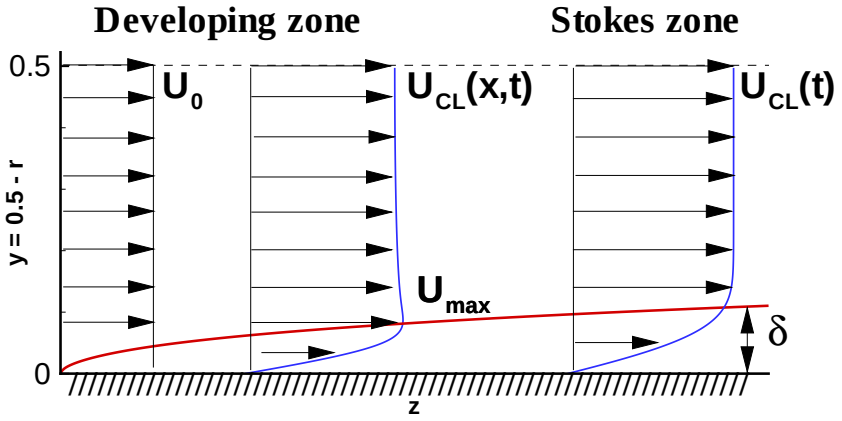

Fig. 3 Sketch of the flow evolution in the inlet region of a circular pipe with uniform entry velocity.

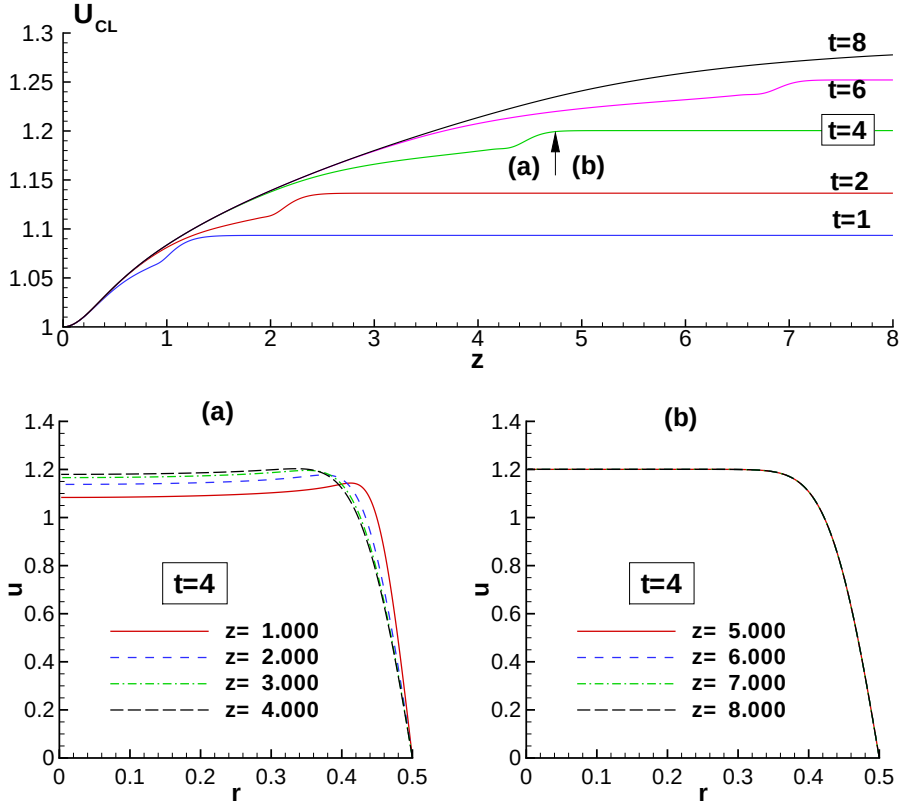

Fig. 4 Pipe-flow simulation for $Re_D = 2500$. Evolution of the centerline velocity U_{CL} versus the axial coordinate z for different time instants. Axial velocity profiles at $t = 4$ showing the separation between (a) the developing flow region ($0 \leq z < 5$) and (b) the Stokes flow region ($5 \leq z \leq 8$).

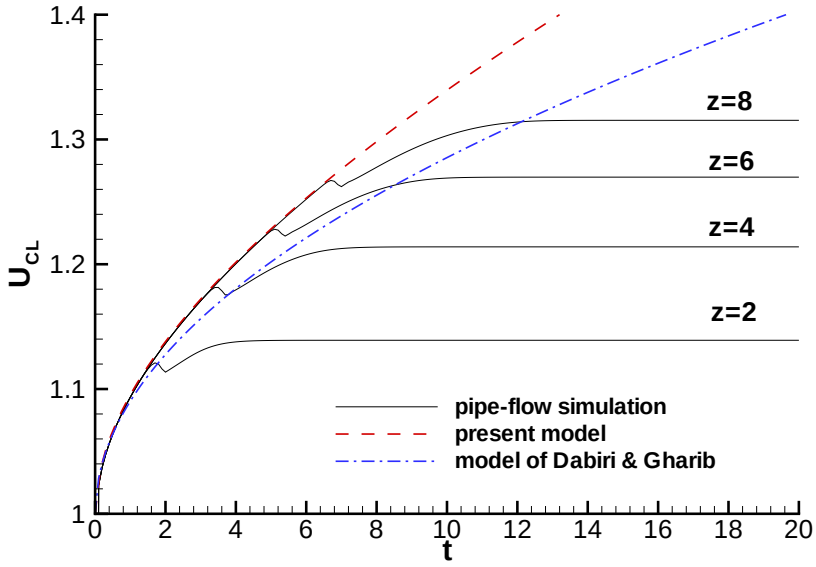

Fig. 5 Pipe-flow simulation for $Re_D = 2500$. Time evolution of the centerline velocity for different streamwise locations and comparison with theoretical models.

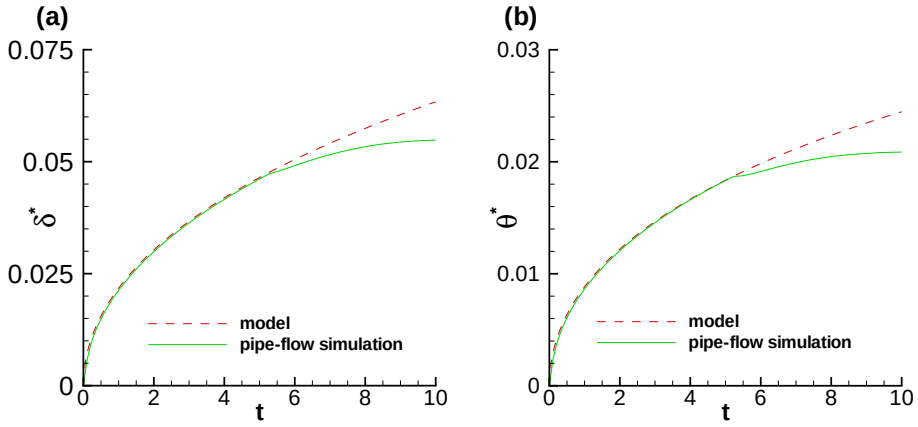

Fig. 6 Pipe-flow simulation for $Re_D = 2500$. Time evolution of the modified displacement (δ^*) and momentum thickness (Θ^*) of the boundary layer in the cross-section located at $z = 6$.

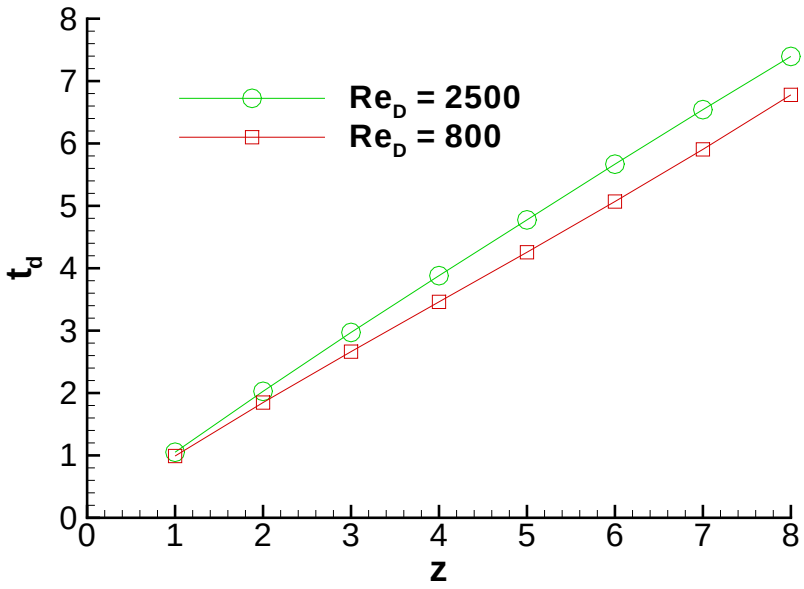

Fig. 7 Pipe-flow simulations for $Re_D = 2500$ and $Re_D = 800$. Validity time-limit of our model for different axial sections: t_d corresponds to a 2% relative error between the model predictions for δ^* and its computation from numerical simulations data (see also Fig. 6).

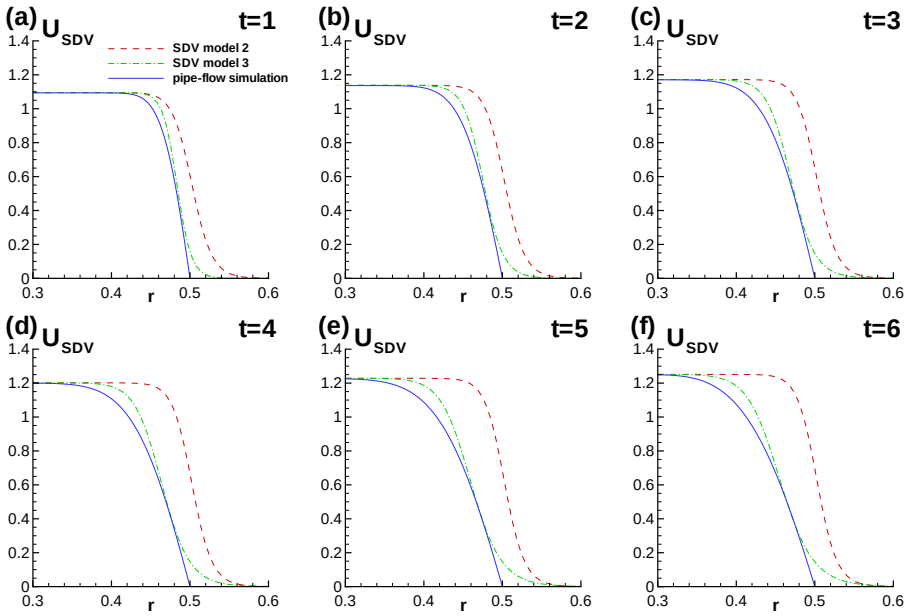

Fig. 8 Velocity profiles at different time instants. Comparison between the profile extracted at $z = 6$ from the pipe-flow numerical simulation with $Re_D = 2500$ (solid line), the SDV model 2 (equation 22) (dashed line) and the SDV model 3 (equation 25) (dash-dot line).

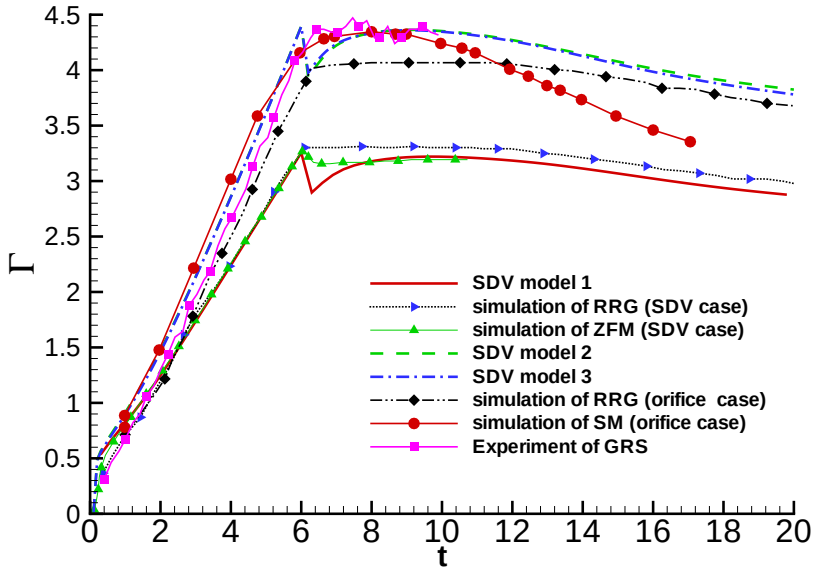

Fig. 9 Vortex ring simulations for $Re_D = 2500$. Time evolution of the total circulation $\Gamma = \widetilde{\Gamma}/(U_0 D)$ for an equivalent piston stroke length $L_P/D = 6$. Present numerical results obtained with SDV models 1, 2, 3 compared to previous numerical (RRG: Rosenfeld, Rambod and Gharib [25], ZFM: Zhao, Frankel and Mongeau [35], SM: Sau and Manesh [28]) and experimental (GRS: Gharib, Rambod and Shariff [8]) results.

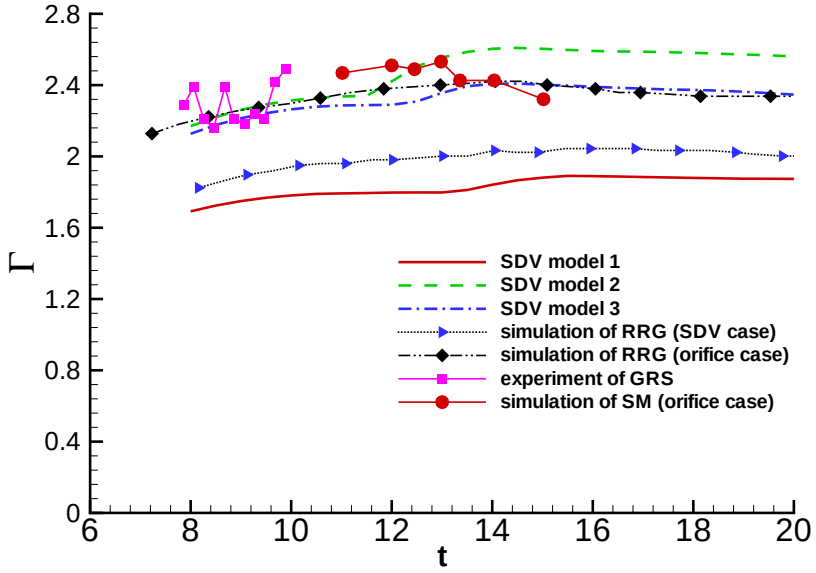

Fig. 10 Vortex ring simulations for $Re_D = 2500$, $L_P/D = 6$. Time evolution of the vortex ring circulation Γ_{VR} (same legend as in Fig. 9).

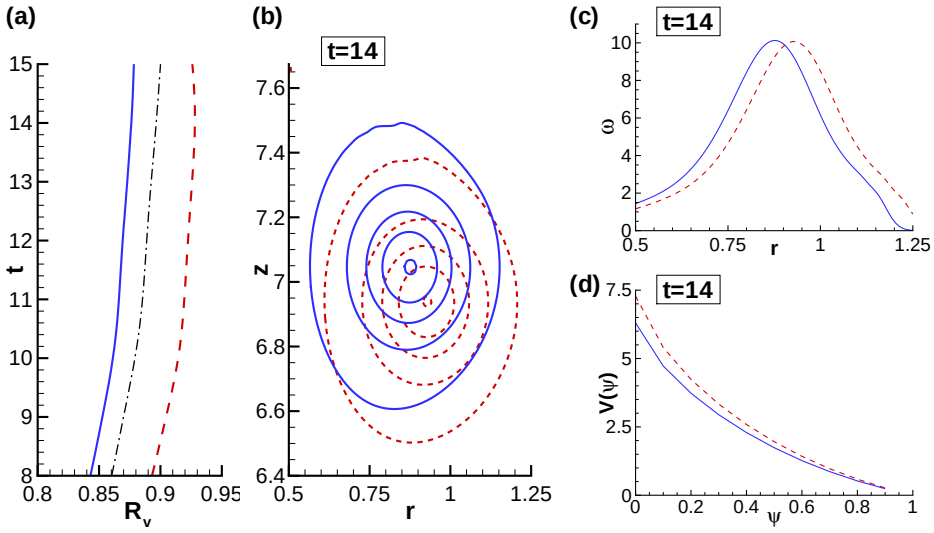

Fig. 11 Vortex ring simulations for $Re_D = 2500$ with SDV model 3 (solid line), model 2 (dashed line) and model 1 (dash-dot line). (a) Time evolution of the radial coordinate R_v of the vortex ring center and characteristics of the vortex ring close to the pinch-off time $t = 14$: (b) iso-contours of the vorticity, (c) radial variation of the vorticity ω along the line passing through the center of the vortex and (d) vortex ring signature $V(\psi)$.

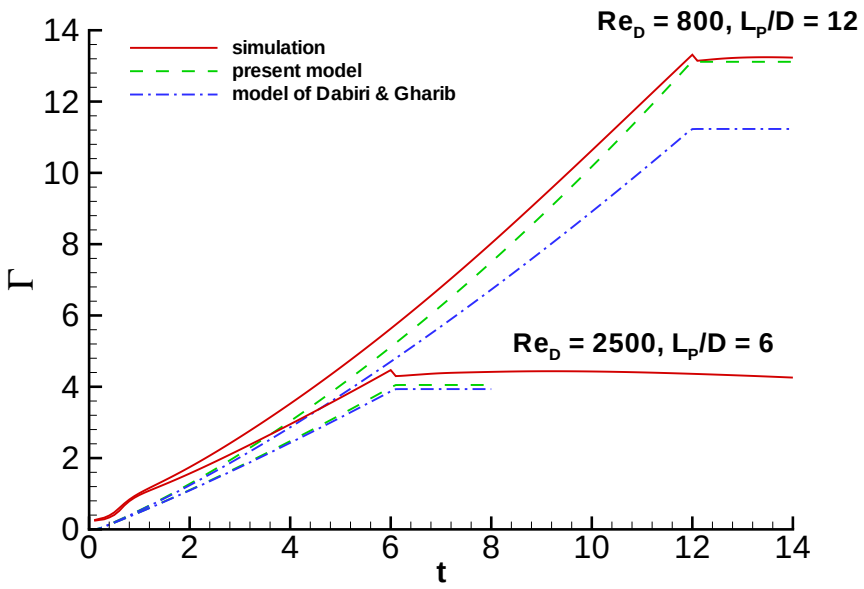

Fig. 12 Vortex ring simulations using at the inflow section velocity profiles from pipe-flow direct numerical simulation. Time evolution of the total circulation (solid line) compared to slug-model prediction using the present model (28)(dashed line) and the model (29) (dash-dot line) corresponding to the centerline correction (21) of Dabiri and Gharib [5] .